

Performance of rice husk ash under different two periods combustion conditions and effect of particle size on the strength of mortar

Z.W. Wang, B.X. Li ✉, A. Othman, Z.B. Zhang

College of Architecture and Environment, Sichuan University, Key Laboratory of Deep Underground Science and Engineering for Ministry of Education, (Chengdu, China)
✉: libix@126.com

Received 24 September 2022
Accepted 13 December 2022
Available on line 21 March 2023

ABSTRACT: This study aims to investigate the effect of two periods burning conditions on the chemical properties of rice husk ash (RHA). Gray correlation theory analysis combined with a scanning electron microscope was used to precisely analyze the impact of RHA particle sizes on the mechanical properties and microstructure of mortar. The experimental results reveal that prolonging residence time at 600 °C could significantly reduce the carbon content and boost the silica content in RHA. The potassium content of RHA could be reduced by burning at a low and then high temperature. Additionally, gray correlation analysis indicated that the particle sizes of 5 -10 µm in RHA could positively accelerate the gaining strength of mortar, followed by 10-15 µm and < 5 µm. At the micro-scale, incorporating RHA with a mean particle of 5.9 µm could accelerate the formation of calcium silicate hydrates having a low Ca/Si by secondary hydration reaction, subsequently leading to the increment of mortar strength.

KEY WORDS: Agricultural byproduct; Rice husk ash; Combustion type; Grey correlation analysis; Supplementary cementitious materials.

Citation/Citar como: Wang, Z.W.; Li, B.X.; Othman, A.; Zhang, Z.B. (2023) Performance of rice husk ash under different two periods combustion conditions and effect of particle size on the strength of mortar. *Mater. Construcc.* 73 [349], e305. <https://doi.org/10.3989/mc.2023.304422>.

RESUMEN: *Comportamiento de la ceniza de cáscara de arroz en diferentes condiciones de combustión de dos periodos y efecto del tamaño de partícula en la resistencia del mortero.* El objetivo de este estudio es investigar el efecto de dos periodos de combustión sobre las propiedades químicas de la ceniza de cáscara de arroz (RHA). Se utilizó el análisis de la teoría de correlación de Gray combinado con un microscopio electrónico de barrido para analizar con precisión el impacto del tamaño de las partículas de RHA en las propiedades mecánicas y la microestructura del mortero. Los resultados experimentales revelan que la prolongación del tiempo de residencia a 600 °C podría reducir significativamente el contenido de carbono y aumentar el contenido de sílice en el RHA. El contenido de potasio del RHA podría reducirse quemándolo a una temperatura baja y luego alta. Además, el análisis de correlación gris indicó que los tamaños de partícula de 5 -10 µm en RHA podrían acelerar la ganancia de resistencias del mortero, seguido por 10-15 µm y < 5 µm. A escala micro, la incorporación de RHA con una partícula tamaño medio de 5,9 µm podría acelerar la formación de hidratos de silicato cálcico con un bajo Ca/Si mediante una reacción de hidratación secundaria, lo que posteriormente conduciría a un aumento de la resistencia del mortero.

PALABRAS CLAVE: Subproducto agrícola; Ceniza de cáscara de arroz; Tipo de combustión; Análisis de correlación de grises; Materiales cementantes suplementarios.

Copyright: ©2023 CSIC. This is an open-access article distributed under the terms of the Creative Commons Attribution 4.0 International (CC BY 4.0) License.

1 INTRODUCTION

Rice husk is an agricultural by-product, in which 20% of the grain is husk, and approximately 20% of the husk is converted to ash after combustion (1). In 2020, the rice production in China was estimated at 211.86 million tons; hence, which can produce about 42.37 million tons of rice husk (2). RHA burnt under 700 °C possess large amounts of amorphous SiO₂ (3-6), which shows high pozzolanic activity and a favorable filling effect. The high pozzolanic activity, that is, amorphous SiO₂ in RHA can react with calcium hydroxide to form secondary hydrate products; moreover, RHA acts as the filling nucleation point for hydration products and refines the pore structure (7), which makes it an ideal supplementary cementitious material (SCM) to effectively enhance mechanical properties (8-12) and durability (13-15) of concrete.

However, the alkali content of RHA was slightly higher than that of fly ash and granulated blast furnace slag, and significantly exceeded that of cement and silica ash (16, 17) required by Chinese standard GB/T 50733-2011 (18), which may induce ASR in mortar or concrete. To address this issue, additional acid treatment before burning could remove the alkali impurities in RHA (19, 20), with the aim of avoiding the ASR of concrete. What needs to be pointed out is that the acid pretreatment methods also increases the production cost and brings secondary chemical pollution to the environment. Therefore, it is essential to explore other measures to reduce the potassium content in RHA.

Sugita S. (21) firstly reported that two periods burning type, in which rice husk was burned at a first lower temperature and then a higher temperature, could be applied to produce RHA with a high silica content, while the influence of carbonization and ashing time on the potassium content of RHA has not been involved. Thereafter, Hongtao Li (22) found that the potassium content of RHA produced at 275 °C for 30 min and then 815 °C for 120 min presented a lower value than that of RHA fabricated at 815 °C for 150 min; and also revealed that the potassium content of RHA showed two situations including a high activity at 275 °C and low activity at 815 °C; however, amorphous SiO₂ in RHA will transfer to crystalline silica at 815 °C. Crucially, R.V. Krishnarao (23) reported that potassium oxide (K₂O) dissociates upon heating at 620 K (347 °C) to form elemental potassium whose melting point is 336.8 K; subsequently, the elemental potassium reacts with carbon composition to form potassium complex compound that is difficult to be released during the combustion process. Therefore, whether prolonging the burning time at a temperature under 620 K (347 °C) could prohibit the transformation from K₂O to potassium complex compound and reduce the potassium con-

tent or not needs to be revealed. Based on these, it is necessary to explore the influence of two periods combustion type on the potassium content of RHA, which could provide proper parameters for manufacturing production.

On the other hand, to achieve the high pozzolanic activity of RHA, RHA should be ground to a fine particle size. Too many researchers only chose several individual particle sizes to initiate comparative analyses. B.H. Abu Bakar (24) examined the influence of fineness levels of RHA varying from 6.65 μm to 17.97 μm on the mechanical properties of concrete, and found that RHA with a median particle size of 9.52 μm could enhance the increment of compressive strength significantly. J. Alex (25) also concluded that the concrete compressive strength increased with RHA fineness modulus decreased; simultaneously, the interfacial transition zone could be enhanced due to the pozzolanic and filling effect of RHA. Moreover, A.P. Vieira (26) compared the mechanical properties of concrete blended RHA with D₅₀ of 7, 14, and 20 μm, respectively, indicating that the compressive strength of concrete increased as RHA particle sizes decreased due to the increasing pozzolanic activity and filling effect. However, it is not enough to determine the optimal particle size of RHA showing the best pozzolanic activity only by comparing several groups of RHA with different average particle sizes, for RHA with a D₅₀ of 6.65 μm presents various RHA particle distributions from 0-100 μm, and it is hardly to mill RHA of a D₅₀ of 6.65 μm with the same particle distribution. Therefore, a more effective and accurate method should be proposed to reveal the optimum particle sizes on the mechanical properties of the concrete or mortar.

This paper focuses on investigating the influence of two periods combustion style on the chemical properties of RHA, especially for the potassium content in RHA, through investigation on the chemical composition, morphology, and crystal pattern of RHA burnt at nine conditions. Meanwhile, grey incidence analysis, a new mathematical model, was conducted to reveal the optimum particle sizes of RHA on the mechanical properties of mortar, and the mechanical test of mortar blended RHA with four different particle sizes was conducted to analyze the influence of each granularity group of RHA on the mortar strength via grey incidence analysis. Additionally, the scanning electron microscope (SEM) and X-ray diffraction (XRD) tests were employed to research the microstructure and composition of hydration products of mortar mixtures and also to reveal the underlying mechanism of the substitution of cement by RHA on the increasing mechanical performance of mortar. Also, the results in this paper are expected to provide references for the industrial production of RHA.

2 MATERIALS AND METHODS

2.1 Materials

Ordinary Portland cement of P•O 42.5R with an average particle size of 13.83 μm was utilized to produce mortar mixes. The chemical oxides composition and loss on ignition (LOI) of cement are presented in Table 1. Chinese ISO standard sand was employed to manufacture mortar, in which the particle size of fine, medium, and coarse sand are 0.08 mm-0.5 mm, 0.5 mm-1 mm, and 1 mm-2 mm, respectively. Raw rice husk was collected from a rice plant in Bengbu (Anhui province, China) and washed, screened, and dried for 24 hours prior to being used in a burning process.

2.2 Experimental program

2.2.1 Combustion experiment

The first study evaluates morphological properties and chemical composition of RHA via two combustion types including straight high temperature (one period) and first lower temperature then higher temperature combustion (two periods), which aims to explore a new burning method to decrease the K₂O content in RHA. The raw rice husk was burnt in a box furnace which could achieve the automatic function of controlling temperature and time. The combustion process contains two key factors, namely the burning temperature

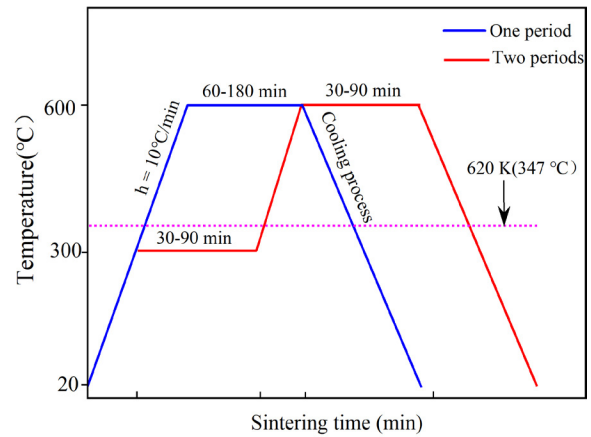


FIGURE 1. Sintering scheme of rice husk.

(300 °C, 600 °C) and residence time (30 min -180 min). In each combustion, rice husk with a mass of 1kg was embedded in the box furnace and then burned according to the set procedure. Nine different schemes were presented in this study as listed in Table 2 and Figure 1.

2.2.2 Mechanical study

A second study was developed to reveal the influence of RHA particle size on the mechanical properties of mortar. RHA produced by L60H120 combustion type was selected and ground for 5 - 30 min in a planetary ball mill at a speed of 60 r/min. The cumulative distribution curve of RHA was measured by laser granulometry (Mode JL-6000) equipment as presented in Figure 2. Due to the

TABLE 1. Chemical composition of cement (wt %).

Materials	SiO ₂	Al ₂ O ₃	Fe ₂ O ₃	CaO	MgO	K ₂ O	Na ₂ O	SO ₃	LOI	Total
Cement	20.24	5.21	3.56	62.47	2.25	-	-	2.58	3.31	99.62

TABLE 2. Calcinations method of rice ash formation by changing temperature and residence time.

Style	Number	Initial temperature	Different sustaining time (min)			
			RT-300 °C	300 °C	300-600 °C	600 °C
One period	L0 H60	RT	h-28	-	h-30	60
	L0 H120	RT	h-28	-	h-30	120
	L0 H180	RT	h-28	-	h-30	180
Two periods	L30 H30	RT	h-28	30	h-30	30
	L30 H60	RT	h-28	30	h-30	60
	L30 H90	RT	h-28	30	h-30	90
	L60 H90	RT	h-28	60	h-30	90
	L90 H90	RT	h-28	90	h-30	90
	L60 H120	RT	h-28	60	h-30	120

Note: RT represents the room temperature. The character of h represents the heating process where the heating rate is 10 °C/min. h-28 and h-30 illustrate that the heating process consumes 28 min and 30 min during RT-300 °C and 300-600 °C, respectively.

chemical properties of RHA were significantly close to silica fume, which also consists of non-crystalline silicon dioxide and high specific surface area. Hence, substituting cement by RHA with four mean particle sizes into mortar was conducted to investigate the pozzolanic activity of RHA in accordance with GB/T 27690 (27). The mixture proportions of mortar are shown in Table 3. The sample names were derived from the mean particle size of RHA. For instance, the sample of RHA35.5 implies that RHA substituted 10% of cement (by mass) with a mean particle size of 35.5 μm. Whereafter, grey correlation analysis was employed to analyze the influencing degree of each group of RHA on the basis of the compressive and flexural strength of mortar.

2.2.3 Grey correlation analysis

In this paper, the interval grey correlation analysis based on the microscopic or macroscopic geometric proximity of the factor sequence was adopted to assess the correlation degree among subsequences and further find an optimum subsequence for impacting the parent sequence (28). In the grey correlation theory, the index column is expressed as $x_m(n)$, where n is the natural number sets, and m is related to the influencing factors. It should be noted that there are l assessment plans in the analysis, i.e., $x_i = [x_i(1), x_i(2), \dots, x_i(n)]$. Meanwhile, parent sequences and subsequences are represented as $x_0 = \{x_0(n)\}$ and $x_i = \{x_i(n)\}$ ($i = 1, 2, \dots, m$), respectively (29). Therefore, the correlation coefficient, $\xi_i(j)$, between subsequence and parent sequence with respect to j^{th} factor could be obtained by Equation [1] (30):

$$\xi_i(j) = \frac{\min_i(\Delta_i \min) + \rho \max_i(\Delta_i \max)}{\Delta_i + \rho \max_i(\Delta_i \max)},$$

$i = 1, 2, \dots, m$ and $j = 1, 2, \dots, n$ [1]

$$\begin{cases} \Delta_i \min = \min_i(|x_0(j) - x_i(j)|) \\ \Delta_i \max = \max_i(|x_0(j) - x_i(j)|) \end{cases} [2]$$

$$\begin{cases} \min_i(\Delta_i \min) = \min_i(|x_0(j) - x_i(j)|) \\ \max_i(\Delta_i \max) = \max_i(|x_0(j) - x_i(j)|) \end{cases} [3]$$

Where Δ_i is equal to $|x_0(j) - x_i(j)|$, ρ is the resolution coefficient, which is to enlarge the difference between the various coefficients within the interval [0, 1]; generally, it is fixed at 0.5 (31). Δ_i and Δ_i denote the minimum and maximum difference in the first level using Equation [2]. Meanwhile, $\max_i(\Delta_i \max)$ and $\min_i(\Delta_i \min)$ are the maximum and minimum difference in the second level, respectively using Equation [3] (29).

Subsequently, the grey correlation degree, r_i , could be obtained from Equation [4] by manipulat-

ing the grey correlation coefficients, which reflect the correlation degree of each subsequence in the same parent sequence. It means that we can find the optimal subsequence by comparing the correlation degree of all subsequences.

$$r_i = \sum_{j=1}^n \xi_i(j) [4]$$

Where $\xi_i(j)$ is the correlation coefficient from Equation [1], and j is within the interval [1, n].

On the other hand, using $\Delta_i = |x_0(j) - x_i(j)|$ calculates the correlation coefficient and correlation polarity including the positive and negative correlation among the subsequence could not be estimated accurately. Hence, in this paper, the judging method of the correlation polarity was defined by a new mathematical way listed in Equation [5], which confirms the correlation including positive and negative correlation from Equation [6] and Equation [7]. The expressions for each of these formulas are shown as follows (32):

$$\begin{cases} \sigma_n = \sum_{i=1}^m x_n(i) \cdot i - \sum_{i=1}^m x_n(i) \cdot \sum_{i=1}^m i/m \\ \sigma_i = \sum_{i=1}^m i^2 - \left(\sum_{i=1}^m i\right)^2 / m \end{cases} [5]$$

$$\text{sgn}\left(\frac{\sigma_i}{\sigma_j}\right) = \text{sgn}\left(\frac{\sigma_k}{\sigma_j}\right), k \in [1, n] [6]$$

$$\text{sgn}\left(\frac{\sigma_i}{\sigma_j}\right) = -\text{sgn}\left(\frac{\sigma_k}{\sigma_j}\right) [7]$$

Where both of σ_n and σ_i are the new defining value, n is the natural number set, and m represents the influencing parent sequence in the analysis. In Equation [6], the value of σ_i overs than zero, while k is within the interval [1, n]. It was noted that subsequence has a positive correlation on enhancing parent sequence when σ_k satisfies the requirement of Equation [6]. Otherwise, a negative correlation that subsequence plays a weakening role on the parent sequence is emerged according to Equation [7].

2.3 Experimental methods

2.3.1 Scanning electron microscope

Scanning electron microscopy (SEM, Helios G4 UC, Japan) with energy-dispersive X-ray (EDX) provided by

TABLE 3. Mix proportions of complex binders.

Sample	Grinding time/min	Content / g				Mean particle size (μm)
		RHA	Cement	ISO sand	Water	
Ref	-	0	450	1350	225	-
RHA35.5	5	45	405	1350	225	35.5
RHA28.2	10	45	405	1350	225	28.2
RHA9.9	15	45	405	1350	225	9.9
RHA5.9	30	45	405	1350	225	5.9

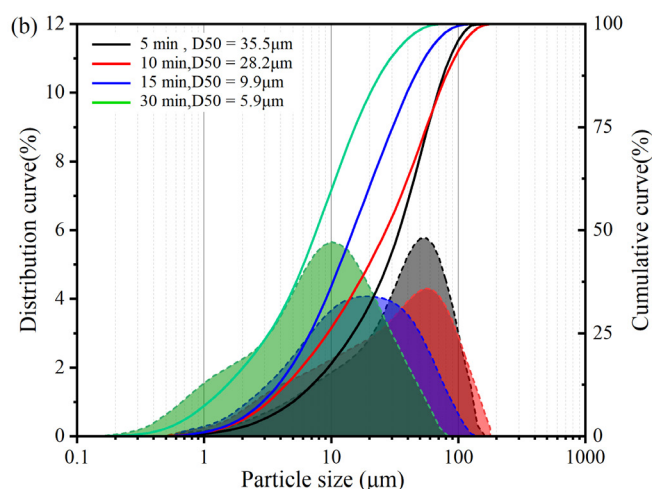


FIGURE 2. Particle size distribution for rice husk ash.

the analytical and testing center of Sichuan University was used to obtain the microstructure of RHA. Moreover, rice husk ash was compacted to a flake layer; thereafter, the surface scan of energy-dispersive X-ray was employed to obtain the accurate chemical elements of RHA samples, as utilized in some previous studies (33, 34).

2.3.2 Mechanical properties

All of the mortar mixtures were bathed into JJ-5 cement and mortar mixer with a 5L capacity. Initially, water was poured into the JJ-5 mixer, then cement and RHA were blended for 120 s throughout the mixing procedure. Then, sand was incorporated slowly and thoroughly mixed for 60 s. Finally, the fresh paste was shaped in the molds and stored with plastic films at the air temperature. After 24 hours, all mortar samples were demolded. The flexural and compressive test complying with GB/T 27690 (27) was conducted on three samples for each mortar mixture. Paste bars having the dimension of 40 mm×40 mm×160 mm were cast. After curing at 65 ± 2 °C for six days and then 21 days in a standard room, all specimens were subject to the compressive and flexural test. Prior to the test, a piece of an unforced segment was cut from the specimens by a saw bar with a thickness of about 0.6 mm

and polished by sanding paper, while the cement hydration process of stores pieces was ceased by isopropyl alcohol and dried in an oven at 60 °C for two hours.

2.3.3 X-ray diffraction

The crystal structure of RHA was measured using an X-ray diffractometer (XRD, EMPYREAN, Holland) operating at an accelerating voltage of 60 kV and 60 mA. Under continuous scanning pattern, Cu K α radiation worked as the source of X-rays, and crystalline phases were scanned from 5° to 80° with a 2 θ increment of 0.02°/step. Although the scanning was performed up to 85° (2 θ), the range of 10 - 50° was analyzed. This is because essential peaks were satisfactorily detected in this range, and meaningful data could not be obtained due to the overlap of peaks at a high angle of > 50° (2 θ).

To obtain the crystal structure of paste samples blended RHA, the hydration of paste samples cured for 28 days was stopped by isopropyl alcohol and dried in an oven at 60 °C for two hours, thereafter, X-ray diffraction was applied after grinding the pieces and passing the sieve of 240 meshes.

3. RESULTS AND DISCUSSION

3.1 Influence of combustion type on morphology and chemical properties of RHA

3.1.1 Morphology

Figure 3 displays the macro-morphology and SEM micrographs of RHA using one period burning method. It can be seen that, as the burning time increases at 600 °C, the black color of RHA tends to change to gray-white. As shown in the SEM micrographs, the scattered particles on the outer surface of RHA present a decreasing development with the increment of high temperature at 600 °C. This phenomenon demonstrates that rice husk biomass such as lignin, cellulose, and spent carbon polymer can be burnt with the increase in the total burning time, which in turn presents a whiter color.

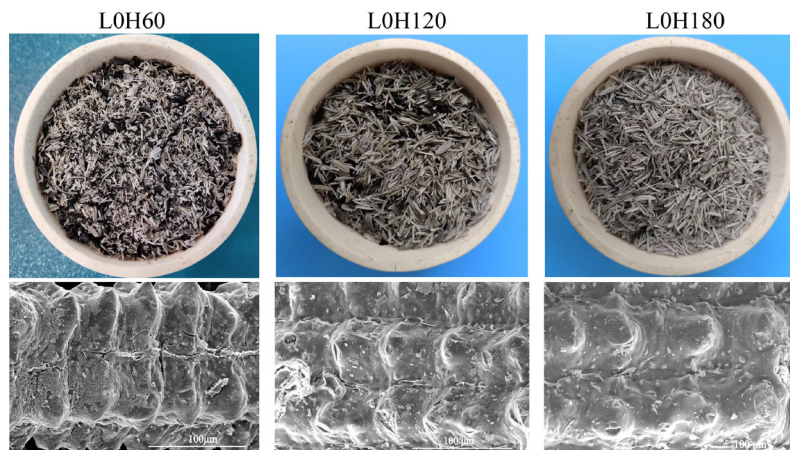


FIGURE 3. Macro-morphology and SEM micrographs of RHA by one period burning methods.

Figure 4 shows the macro-morphology and SEM micrographs of RHA by two periods burning methods. Similarly, the white color of RHA tends to enhance as the total burning time increases; however, RHAs produced in L60H90, L90H90, and L60H120 appear remarkably similar gray-white color, which is possible due to the reducing biomass which could be wholly oxidized and then burnt when the burning

time was up to 90 min at 600 °C. This perspective could be certified by the low carbon content in Table 5. From the SEM micrographs, massive granular impurities are attached on the outer surface of RHA in L30H30 due to the insufficient combustion time. The scattered particles on the outer surface of RHA present a rapidly decreasing tendency as the total burning time increases.

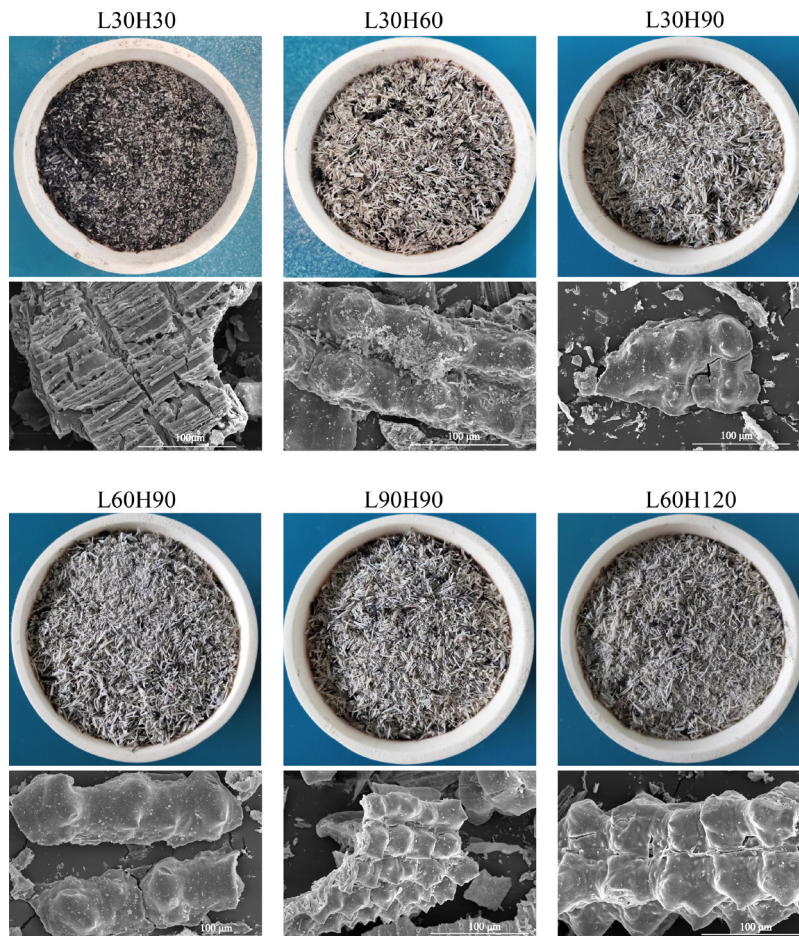


FIGURE 4. Macro-morphology and SEM micrographs of RHA by two periods burning methods.

3.1.2 X-ray diffraction analysis

The XRD patterns of RHA by nine burning methods are presented in Figure 5. It could be seen that all samples emerge no noticeable sharp peak from the diffraction curve. Besides, a hump at 2θ -near 15° - 25° could be observed, which confirms the presence of amorphous silica in terms of the qualitative assessment of RHA. Previous researchers, who explored the varied temperature to the influence on the crystallinity of silica in RHA from XRD patterns, also found that amorphous silica could be obtained and untransformed to crystalline silica such as cristobalite and tridymite using temperature lower than 700°C , which was is responsible for the critical pozzolanic activity of RHA (35, 36).

3.1.3 Chemical composition

In this study, a semi-quantitative method, energy-dispersive X-ray, was used to determine the chemical composition of RHA, as listed in Table 4. From Table 4, in one period, the carbon content of RHA could be noticeably reduced when the total burning time at 600°C increased from 60 min to 120 min; meanwhile, the silica content of RHA also could noticeably increase. In two periods, the carbon content of RHA in L30H60 could be noticeably decreased by 86.5% compared with that of RHA in L30H30. Moreover, the silica content of RHA increased rapidly by prolonging the high temperature stage in L30H30, L30H60, and L30H90. However, the silica content of RHA by extending the low temperature stage in L30H90, L60H90, and L90H90 has an insignificant variation, indicating that it was hard to increase when the burning time at 600°C was up to 90 min.

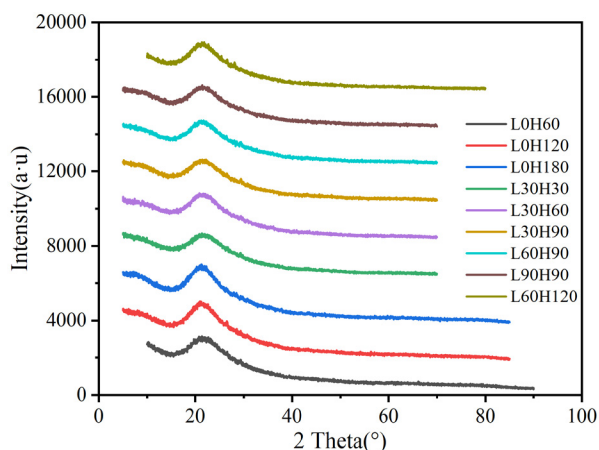


FIGURE 5. XRD patterns of rice husk ash in different burning implementations.

Figure 6 shows the potassium and silica content in RHA with different combustion types. It is ob-

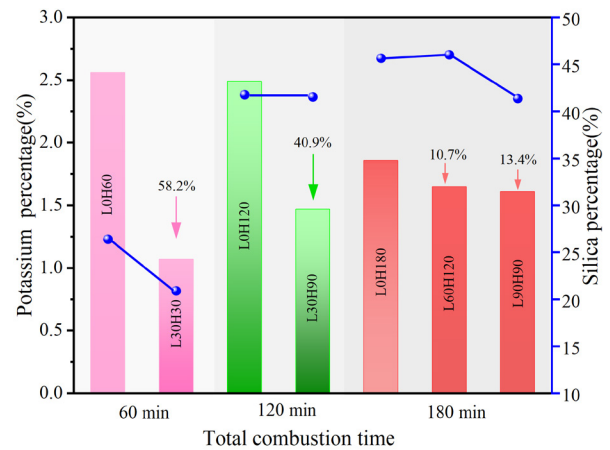


FIGURE 6. Potassium content in RHA by EDX analysis.

served in Figure 6 that the potassium content in RHA generated by one period decreased by 58.2%, 40.9%, and 12.3% (average value), respectively, compared to the potassium of RHA produced by two periods that the total burning time was 60 min, 120 min, and 180 min, respectively. This phenomenon indicates that increasing combustion time at a low temperature of 300°C could reduce potassium content when total combustion time was constant. Two patterns of potassium were presented in RHA: potassium oxide and potassium complex compound. Potassium oxide in RHA could be dissociated to potassium when the temperature exceeds 620 K (347°C) (23), thereafter the potassium reacts with other elements to form a potassium complex compound that could fix carbon to form black particles in RHA, thus resulting in a high potassium content in RHA. Hence, prolonging the low temperature at 300°C under 620 K could reduce the formation of black particles in RHA; meanwhile, potassium whose melting point is 336.8 K could fully evaporate accompanied by carbon in RHA as the combustion time increases at 300°C . On the other hand, RHA straightly burnt from room temperature to 600°C contributes to a longer combustion time above 620 K (347°C), thus forming a more potassium complex compound and maintaining a high potassium content in RHA. However, the decreasing potassium content of RHA in L90H90 and L60H120 was not noticeable compared to that of RHA in L0H180. Moreover, the potassium content of RHA in L30H90, L60H90, and L90H90 was 1.47%, 0.93%, and 1.61%, respectively, which implied that a longer time at 300°C than 60 min could not always motivate the evaporation of potassium accompanied by carbon due to the restricted oxygen in the furnace which was supplied from the outside air in this study. Hence, a reasonable low-temperature stage should be applied to effectively reduce the potassium content in RHA.

On the other hand, considering the amorphous silica and potassium content as well as the energy consumption among nine burning types, L60H90 presents a lower potassium content and electric energy consumption than L90H90 and L60H120. However, L60H120 has a greater silica content; meanwhile, the equivalent alkalis content of RHA in L60H120 was 1.33% by transforming the potassium to corresponding oxides, which was lower than 2.5% of fly ash and 1.5% of silica ash per GB/T 50733-2011 (16). To ensure the high pozzolanic activity of RHA, L60H120 with a superior silica content was selected in this paper.

3.2 Influence of RHA particle size on mechanical properties of mortar

3.2.1 Pozzolanic activity

The pozzolanic activity of RHA produced by L60H120 was investigated according to GB/T 27690 (27). The flexural and compressive strength of mortar containing RHA with four varying particle sizes at 7 and 28 days are plotted in Figure 7 and Figure 8, respectively. Also, the pozzolanic activity index of RHA is presented in Figure 8.

As can be seen, as RHA particle size decreases, substituting cement by RHA noticeably increases the compressive strength of mortar, while the flexural strength of mortar was slightly improved. Furthermore, the pozzolanic activity index of RHA increases as its particle size decreases since finer RHA opposes higher specific surface area, which can provide more nucleation sites for cement hydration, thus facilitating the pozzolanic reaction of RHA to form more C-S-H having a low Ca/Si and fill the pores of mortar (37, 38).

Figure 8 illustrates that the pozzolanic activity index of RHA milled from 5 min to 30 min are

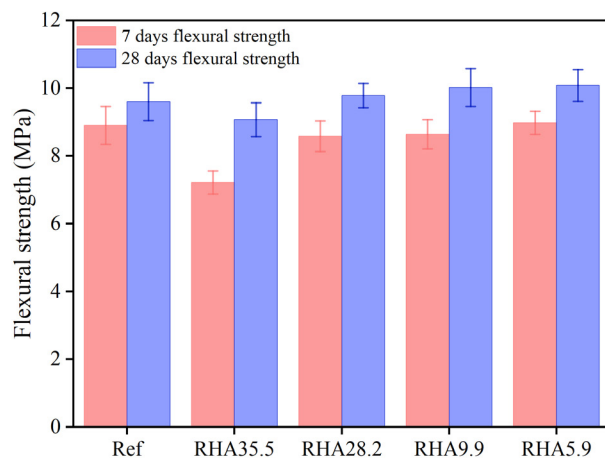


FIGURE 7. Effect of RHA on flexural strength of complex pastes.

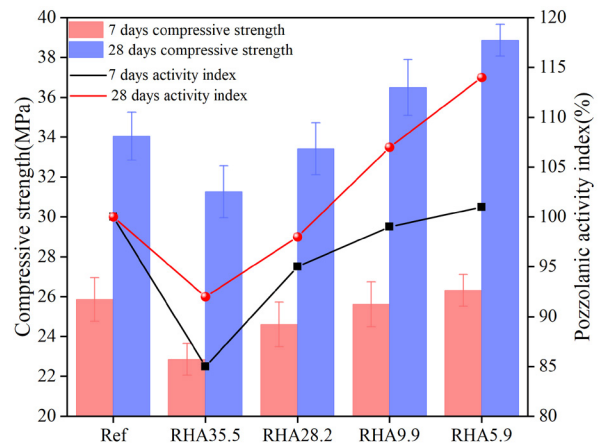


FIGURE 8. Effect of RHA on compressive strength and pozzolanic activity index of complex pastes.

85%, 95%, 99%, and 101% at 7 days, respectively. The curing days have a significant influence on the hydration degree of cement, which found that the pozzolanic activity indexes of RHA are up to 92%, 98%, 107%, and 114% at 28 days, respectively. It can be obtained that all pozzolanic activity indexes of RHA at 7 days are lower than 105%, which does not conform to the prescriptive value of silica fume in accordance with GB/T 27690 (27). However, the activity index of RHA at 28 days meets the requirement that the activity index of silica fume should be greater than 85% complying with GB/T 51003 (39). Therefore, it can be inferred that the particle size of RHA should reasonably vary from 15 min to 30 min to meet its requirement of pozzolanic activity, which contributes the particle packing effect and pozzolanic effect to enhance the mortar strength.

3.2.2 Correlation analysis between RHA particle size and mortar strength

As listed in Table 5, the flexural and compressive strength of mortar at 7 and 28 days are presumed as parent sequences by $X_{01}(n)$, $X_{02}(n)$, $X_{03}(n)$ and $X_{04}(n)$, respectively. Moreover, the particle size system of RHA is cut apart into six subsequences including $<5 \mu\text{m}$, $5\text{-}10 \mu\text{m}$, $10\text{-}15 \mu\text{m}$, $15\text{-}20 \mu\text{m}$, $20\text{-}45 \mu\text{m}$ and $>45 \mu\text{m}$, which were defined by $X_1(n)$, $X_2(n)$, ..., $X_6(n)$, respectively (as listed in Table 6).

The correlation degree and polarity between the subsequences and parent sequences were analyzed by grey correlation analysis as summarized in Table 7. It can be observed that, overall, during the six subsequences, the correlation degree of four subsequences emerges as a consistent developing rule that contains the same arranging order. Meanwhile, the particle size of $15 \mu\text{m}$ is a critical factor in determining the correlation polarity in different subsequences. From Table 7, in terms of correlation polarity, the particle size below $15 \mu\text{m}$ in RHA

TABLE 4. Chemical composition of RHA by EDX (wt %) analysis and LOI of RHA.

styles	Number	C	O	Na	Mg	Al	Si	P	S	Cl	Ca	Fe	K	LOI*
One period	L0H60	28.09	41.67	0.07	0.14	0.04	26.39	0.13	0.11	0.08	0.36	0.35	2.56	24.5
	L0H120	4.53	49.85	0.03	0.00	0.10	41.77	0.17	0.00	0.13	0.89	0.03	2.49	10.4
	L0H180	5.60	45.26	0.00	0.09	0.00	45.63	0.64	0.42	1.86	0.38	0.13	1.86	7.2
Two periods	L30H30	39.56	37.85	0.06	0.12	0.04	20.90	0.07	0.04	0.00	0.30	0.00	1.07	27.2
	L30H60	5.34	53.19	0.05	0.07	0.17	38.91	0.00	0.06	0.08	-	0.27	1.86	11.4
	L30H90	5.52	49.62	0.02	0.23	0.09	41.52	0.17	0.30	0.13	0.88	0.03	1.47	5.31
	L60H90	4.85	53.17	0.04	0.19	0.09	40.10	0.17	0.11	0.09	0.25	0.04	0.93	4.93
	L90H90	3.34	52.58	0.07	0.09	0.13	41.36	0.08	0.07	0.08	0.41	0.18	1.61	4.28
	L60H120	2.66	48.26	0.05	0.12	0.06	46.03	0.15	0.06	0.18	0.54	0.24	1.65	4.5

*LOI: loss on ignition

can have a positive influence on promoting the strength development of mortar. According to the correlation degree of six subsequences, the particle size of 5-10 μm in RHA contributes mostly to the strength development, followed by 10-15 μm and <5 μm . Analyzed by the above value of correlation degree, a smaller particle size of < 5 μm is inconsistent with the conclusion that the finer particle of RHA contributes to the higher pozzolanic reaction. That is possible because of the increase of grinding degree, which destroys some pore structures of RHA particles, thus inducing the porous microstructure to collapse and partially break into finer ones (40).

On the other hand, using RHA with a particle size exceeding 15 μm could result in a negative correlation

on the strength of mortar complying with correlation polarity analysis. The largest negative effect of particle sizes will be reflected when the particle size of RHA is greater than 45 μm , followed by 0-45 μm and 15 μm -20 μm in accordance with the correlation degree of six subsequences. Hereby, the grinding time of raw RHA should be reasonably controlled in 15-30 min to improve the particle content under 15 μm in RHA and significantly reduce the particle content above 45 μm .

3.2.3 Microstructure

The microstructure of Ref and RHA5.9 samples analyzed by scanning electron microscope (SEM)

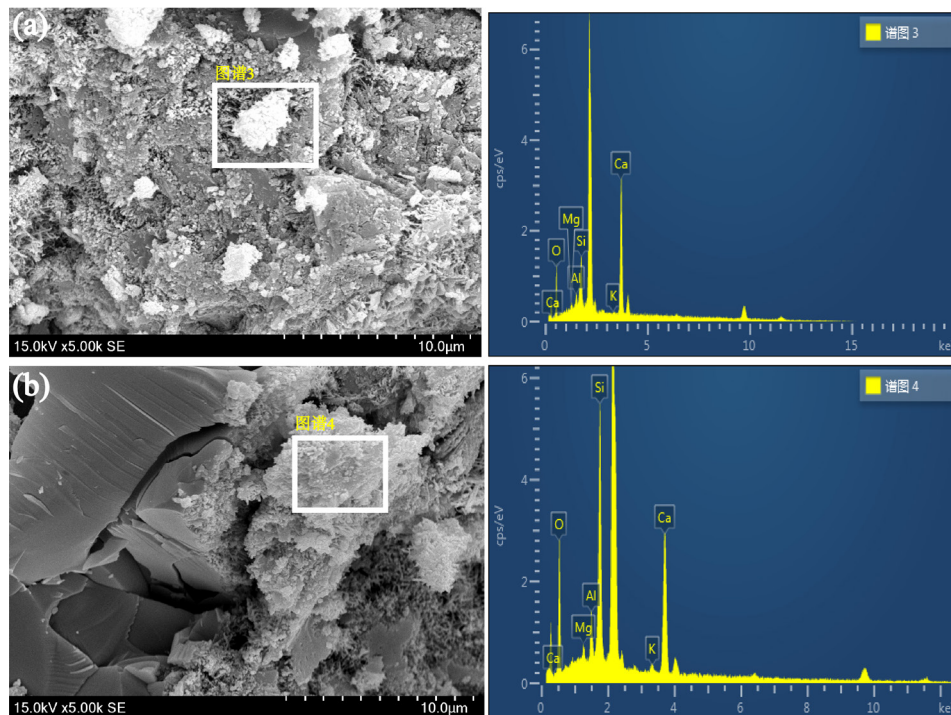


FIGURE 9. SEM-EDX micrograph of (a) Ref paste and (b) RHA5.9 paste.

and energy-dispersive X-ray (EDX) are illustrated in Figure 9 and Figure 10. The chemical composition of hydrates products is listed in Table 8. The atom ratio of Ca/Si in hydrates products decreased from 5.88 to 1.03 when cement was replaced by RHA with a mean particle size of 5.9 μm , indicating that using RHA substitute cement contributed to the pozzolanic reaction of RHA, thus forming a new C-S-H gel that its Ca/Si is lower than 1.5 and presents a fibrous gel of fine C-S-H (I) (41). Furthermore, from Figure 10. It could be observed that the peak intensity of portlandite (2θ =near 18°) in Ref was higher than that of portlandite in the RHA5.9, indicating that RHA with a mean particle size of 5.9 μm presented a superior pozzolanic activity. Additionally, incorporating RHA weakened the peak intensity of ettringite (2θ =near 9°), which also indicates that RHA accurate the hydration degree of cement.

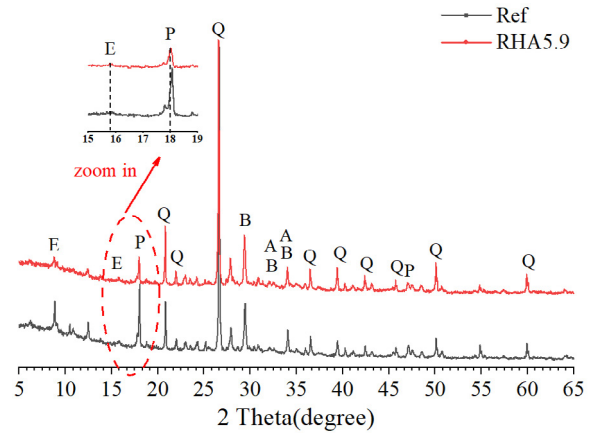


FIGURE 10. XRD patterns of the mixtures (A:Alite- C_3S ; B:-Belite- C_2S ; E:Ettringite-AFt; Q:Quartz- SiO_2 ; P:Portlandite- $\text{Ca}(\text{OH})_2$).

TABLE 5. Parent sequences.

Sample	$X_{01}(n)$ Flexural strength 7d/MPa	$X_{02}(n)$ Compressive strength 7d/MPa	$X_{03}(n)$ Flexural strength 28d/MPa	$X_{04}(n)$ Compressive strength 28d/MPa
RHA35.5	7.22	22.85	9.07	31.26
RHA28.2	8.58	24.61	9.78	33.42
RHA9.9	8.64	25.61	10.02	36.49
RHA5.9	8.98	26.31	10.08	38.86

Note: all of the $X_{01}(n)$ 、 $X_{02}(n)$ 、 $X_{03}(n)$ and $X_{04}(n)$ belong to the parent sequences of $\{X_0(n)\}$.

TABLE 6. Subsequences.

Sample	$X_1(n)/\%$ ($<5 \mu\text{m}$)	$X_2(n)/\%$ ($5-10 \mu\text{m}$)	$X_3(n)/\%$ ($10-15 \mu\text{m}$)	$X_4(n)/\%$ ($15-20 \mu\text{m}$)	$X_5(n)/\%$ ($20-45 \mu\text{m}$)	$X_6(n)/\%$ ($>45 \mu\text{m}$)
A1	8.43	9.25	8.73	5.45	30.47	37.68
A2	14.39	11.94	9.95	5.59	24.68	33.45
A3	39.13	10.99	13.08	5.13	25.46	6.26
A4	47.96	11.75	13.45	5.03	18.52	3.31

Note: all of the $X_1(n)$ 、 $X_2(n)$ 、...、 $X_6(n)$ belong to the parent sequences of $\{X_i(n)\}$, $i \in [1,6]$ and $n \in [1,4]$.

TABLE 7. Correlation degree and correlation polarity.

Particle size	$<5 \mu\text{m}$	$5-10 \mu\text{m}$	$10-15 \mu\text{m}$	$15-20 \mu\text{m}$	$20-45 \mu\text{m}$	$>45 \mu\text{m}$
7d Flexural strength	(+) 0.512	(+) 0.957	(+) 0.827	(-) 0.863	(-) 0.794	(-) 0.405
7d Compressive strength	(+) 0.504	(+) 0.917	(+) 0.811	(-) 0.868	(-) 0.816	(-) 0.402
28d Flexural strength	(+) 0.492	(+) 0.903	(+) 0.789	(-) 0.881	(-) 0.817	(-) 0.399
28d Compressive strength	(+) 0.541	(+) 0.921	(+) 0.875	(-) 0.851	(-) 0.804	(-) 0.412

Note: the sign of “+” and “-” present the positive and negative effects on the strength of mortar.

TABLE 8. EDX element analysis of hydrate products.

Mixtures	Element	O	Mg	Al	Si	K	Ca	Ca/Si
Ref	At%	58.14	1.01	2.02	5.60	0.34	32.90	5.88
RHA5.9		58.94	1.19	3.80	17.41	0.82	17.84	1.03

4 DISCUSSION

In this paper, using two periods burning condition could effectively decrease the potassium content of RHA to a certain extent compared to one period burning process, which is a new finding. The design idea was original from R.V. Krishnarao (23), which reported that potassium oxide in RHA could be dissociated with potassium when the temperature exceeds 620 K (347°C). Thereafter, the dissociated potassium react with other substance to form potassium complex compound which is hard to be removed at a high temperature. Therefore, prolonging the low temperature under 347 °C could reduce the transferred potassium complex compound and contribute to the release of K₂O. However, the decreasing degree of potassium content in RHA was gradually weakened as the burning time increased. This is possible due to the fact that more time than 60 min at 300 °C could not motivate the evaporation of potassium accompanied by carbon due to the restricted oxygen in the furnace which was supplied from the outside air in this study. Hence, a firing device should be developed to contribute to the effective combustion process in the future. Overall, two periods combustion type of rice hush is promising to reduce the potassium content in RHA.

In general, finer RHA possesses higher pozzolanic activity. The precise optimal particle size of RHA contributed to the gaining strength has not been reported in previous studies. Actually, RHA with an average particle size of 5.9-35.5 µm was composited by various particles ranging from 0-100 µm where fine particles show high pozzolanic activity, and coarse particles only show the filling effect and low pozzolanic activity. In this paper, correlation analysis could judge the influence of various particles in RHA on its pozzolanic activity. The particle size less than 15 µm in RHA positively promotes the mortar strength development, especially in the optimal particle group (5-10 µm).

5 CONCLUSIONS

In this paper, nine combustion types were employed to investigate the influence on the morphology, chemical composition, and crystallinity of RHA due to different combustion modes. Moreover, the influence of particle size distribution of RHA on the

strength of mortar was also explored by using grey correlation analysis and strength testing. The special conclusions can be drawn as follows:

(1) An optimum processing technic of RHA as SCM was proposed, including combustion type L60H120 and particle size zone (5-10 µm).

(2) The amorphous silica content of RHA can be up to 91% and carbon content of declines sharply when using L60H120.

(3) The pozzolanic activity index of RHA critically depends on RHA particle size, and RHA containing a median particle size of 5.9 µm presents much better pozzolanic activity index of 101 % and 114 % than the other three RHAs at 7 and 28 curing days, respectively.

(4) The improving mechanism of mortar by adding RHA includes both combined packing effect and pozzolanic reaction of RHA, and the substitution of cement by RHA contributes to the pozzolanic reaction to form C-S-H having a low Ca/Si, which results in the significant gaining strength of mortar.

ACKNOWLEDGMENTS

The authors would like to graciously thank the National Nature Science Foundation of China (Grant No. 51678379) for the financial support of this work.

AUTHOR CONTRIBUTIONS:

Conceptualization: Z.W. Wang. Data curation: Z.W. Wang. Formal analysis: Z.W. Wang. Funding acquisition: B.X. Li. Investigation: Z.W. Wang, B.X. Li, A. Othman, Z.B. Zhang. Methodology: Z.W. Wang. Project administration: B.X. Li. Resources: B.X. Li. Supervision: B.X. Li. Visualization: Z.W. Wang, A. Othman. Writing, original draft: Z.W. Wang.

REFERENCES

- Givi, A.N.; Rashid, S.A.; Aziz, F.N.; Salleh, M.A. (2010) Assessment of the effects of rice husk ash particle size on strength, water permeability and workability of binary blended concrete. *Constr. Build. Mater.* 24 [11], 2145–2150. <https://doi.org/10.1016/j.conbuildmat.2010.04.045>.
- National Bureau of Statistics. Announcement of the National Bureau of statistics on grain production data in 2020. [online] Retrieved from http://www.stats.gov.cn/tjsj/zxfb/202012/t20201210_1808377.html. [Accessed: 10 Oct 2020].
- Deshmukh, P.; Bhatt, J.; Peshwe, D.; Pathak, S. (2012) Determination of silica activity index and XRD, SEM and EDS studies of amorphous SiO₂ extracted from rice husk ash. *T. Indian I. Metals.* 65 [1], 63-70. <https://doi.org/10.1007/s12666-011-0071-z>.
- Sarang, M.; Nayak, P.; Tiwari, T.N. (2011) Effect

- of temperature on nano-crystalline silica and carbon composites obtained from rice-husk ash. *Compos. Part B-Eng.* 42 [7], 1994-1998. <https://doi.org/10.1016/j.compositesb.2011.05.026>.
5. Kang, S.H.; Hong, S.G.; Moon, J. (2019) The use of rice husk ash as reactive filler in ultra-high performance concrete. *Cem. Concr. Res.* 115, 389-400. <https://doi.org/10.1016/j.cemconres.2018.09.004>.
 6. Villaquiran-Cacedo, M.A.; de Gutierrez, R.M.; Gallego, N.C. (2017) A novel MK-based geopolymer composite activated with rice husk ash and KOH: Performance at high temperature. *Mater. Construcc.* 67 [326]. <https://doi.org/10.3989/mc.2017.02316>.
 7. Rodriguez de Sensale, G. (2010) Effect of rice-husk ash on durability of cementitious materials. *Cem. Concr. Comp.* 32 [9], 718-725. <https://doi.org/10.1016/j.cemconcomp.2010.07.008>.
 8. Zhang, Z.G.; Yang, F.; Liu, J.C.; Wang, S.P. (2020) Eco-friendly high strength, high ductility engineered cementitious composites (ECC) with substitution of fly ash by rice husk ash. *Cem. Concr. Res.* 137, 106200. <https://doi.org/10.1016/j.cemconres.2020.106200>.
 9. Bheel, N.; Keerio, M.A.; Kumar, A.; Shahzaib, J.; Ali, Z.; Ali, M.; Sohu, S. (2021) An investigation on fresh and hardened properties of concrete blended with rice husk ash as cementitious ingredient and coal bottom ash as sand replacement material. *Silicon-Neth.* 14 [2], 677-688. <https://doi.org/10.1007/s12633-020-00906-3>.
 10. Intaboot, N. (2020) Innovation of interlocking block mixing with biomass for sound absorption and thermal conductivity in Thailand. *J. Adv. Concr. Technol.* 18 [8], 473-480. <https://doi.org/10.3151/jact.18.473>.
 11. Pavia, S.; Aly, M. (2016) Influence of aggregate and supplementary cementitious materials on the properties of hydrated lime (CL90s) mortars. *Mater. Construcc.* 66 [324], e104. <https://doi.org/10.3989/mc.2016.01716>.
 12. Tashima, M.M.; Soriano, L.; Monzó, J.; Borrachero, M.V.; Akasaki, J.L.; Payá, J. (2014) New method to assess the pozzolanic reactivity of mineral admixtures by means of pH and electrical conductivity measurements in lime:pozzolan suspensions. *Mater. Construcc.* 64 [316], e032. <https://doi.org/10.3989/mc.2014.00914>.
 13. Peng, G.F.; Yang, J. (2016) Influence of rice husk ash on the properties of concrete: a review. In: International forum on energy, environment and sustainable development (IFEESD) *Shenzhen Peoples R. China.* 143-149.
 14. Pradhan, B. (2014) Corrosion behavior of steel reinforcement in concrete exposed to composite chloride-sulfate environment. *Constr. Build. Mater.* 72, 398-410. <https://doi.org/10.1016/j.conbuildmat.2014.09.026>.
 15. Antiohos, S.K.; Tapali, J.G.; Zervaki, M.; Sousa-Coutinho, J.; Tsimas, S.; Papadakis, V.G. (2013) Low embodied energy cement containing untreated RHA: A strength development and durability study. *Constr. Build. Mater.* 49, 455-463. <https://doi.org/10.1016/j.conbuildmat.2013.08.046>.
 16. Wang, J.; Xiao, J.; Zhang, Z.; Han, K.; Hu, X.; Jiang, F. (2021) Action mechanism of rice husk ash and the effect on main performances of cement-based materials: A review. *Constr. Build. Mater.* 288, 123068. <https://doi.org/10.1016/j.conbuildmat.2021.123068>.
 17. Zhu, H.J.; Liang, G.W.; Xu, J.; Wu, Q.S.; Zhai, M.N. (2019) Influence of rice husk ash on the waterproof properties of ultrafine fly ash based geopolymer. *Constr. Build. Mater.* 208, 394-401. <https://doi.org/10.1016/j.conbuildmat.2019.03.035>.
 18. GB/T 50733-2011 (2011) Technical code for prevention of alkali-aggregate reaction in concrete. Standards Press of China, Beijing, China.
 19. Zhang, H.X.; Zhao, X.; Ding, X.F.; Lei, H.; Chen, X.; An, D.M.; Li, Y.L.; Wang, Z.C. (2010) A study on the consecutive preparation of D-xylose and pure superfine silica from rice husk. *Bioresour. Technol.* 101 [4], 1263-1267. <https://doi.org/10.1016/j.biortech.2009.09.045>.
 20. Ma, X.Y.; Zhou, B.; Gao, W.; Qu, Y.N.; Wang, L.L.; Wang, Z.C.; Zhu, Y.C. (2012) A recyclable method for production of pure silica from rice hull ash. *Powder Technol.* 217, 497-501. <https://doi.org/10.1016/j.powtec.2011.11.009>.
 21. Sugita, S. (1996) Fundamental study on the effective utilization of rice husk ash as concrete materials. Hokkaido: Hokkaido University.
 22. Li, H.B.; Li, B.X.; Xu, Y.N.; Gao, X.Y. (2013) Effect of calcination method on morphological characteristics and composition of rice husk ash. *Trans. Chin. Soc. Agric. Mach.* 44 [4], 131-136. <https://doi.org/10.6041/j.issn.1000-1298.2013.04.024>. (in Chinese).
 23. Krishnarao, R.V.; Subrahmanyam, J.; Kumar, T.J. (2001) Studies on the formation of black particles in rice husk silica ash. *J. Eur. Ceram. Soc.* 21 [1], 99-104. [https://doi.org/10.1016/S0955-2219\(00\)00170-9](https://doi.org/10.1016/S0955-2219(00)00170-9).
 24. Abu Bakar, B.H.; Azmi, M.J.M.; Ramadhansyah, P.J. (2011) Effect of rice husk ash fineness on the chemical and physical properties of concrete. *Mag. Concr. Res.* 63 [5], 313-320. <https://doi.org/10.1680/macrc.10.00019>.
 25. Alex, J.; Dhanalakshmi, J.; Ambedkar, B. (2016) Experimental investigation on rice husk ash as cement replacement on concrete production. *Constr. Build. Mater.* 127, 353-362. <https://doi.org/10.1016/j.conbuildmat.2016.09.150>.
 26. Vieira, A.P.; Toledo, R.D.; Tavares, L.M.; Cordeiro, C.C. (2020) Cordeiro. Effect of particle size, porous structure and content of rice husk ash on the hydration process and compressive strength evolution of concrete. *Constr. Build. Mater.* 236, 117553. <https://doi.org/10.1016/j.conbuildmat.2019.117553>.
 27. GB/T 27690-2011 (2011) Silica fume for cement mortar and concrete. Standardization Administration of China Beijing, China.
 28. Feng, Y.X.; Hong, Z.X.; Cheng, J.; Jia, L.K.; Tan, J.R. (2017) Low carbon-oriented optimal reliability design with interval product failure analysis and grey correlation analysis. *Sustainability-Basel.* 9 [3], 369-383. <https://doi.org/10.3390/su9030369>.
 29. Li, H.H.; Chen, D.Y.; Arzaghi, E.; Abbassi, R.; Xu, B.B.; Patelli, E.; Tolo, S. (2018) Safety assessment of hydro-generating units using experiments and grey-entropy correlation analysis. *Energy.* 165, 222-234. <https://doi.org/10.1016/j.energy.2018.09.079>.
 30. Wang, W.P.; Yang, Z.M.; Lu, Y.; Sin, Y.L.; Zhang, B. (2015) The optimization degree of provincial industrial ecosystem and EKC of china-based on the grey correlation analysis. In: Proceedings of 2015 (IEEE) International Conference on Grey Systems and Intelligent Services (GSIS), Leicester, United Kingdom. 179-186.
 31. Chiang, K.T.; Chang, F.P. (2006) Optimization of the WEDM process of particle-reinforced material with multiple performance characteristics using grey relational analysis. *J. Mater. Process. Tech.* 180 [1-3], 96-101. <https://doi.org/10.1016/j.jmatprotec.2006.05.008>.
 32. Deng, J. (1990) A course in grey systems theory. Press of Huazhong University of Science and Technology, Wuhan, China, 1990. (in Chinese).
 33. Li, H.; Li, B.; Xu, Y.; Gao, X. (2013) Effect of calcination method on morphological characteristics and composition of rice husk ash. *Trans. Chin. Soc. Agric. Mach.* 44 [4], 131-136. <https://doi.org/10.6041/j.issn.1000-1298.2013.04.024>.
 34. Bie, R.S.; Song, X.F.; Liu, Q.Q.; Ji, X.Y.; Chen, P. (2015) Studies on effects of burning conditions and rice husk ash (RHA) blending amount on the mechanical behavior of cement. *Cem. Concr. Compos.* 55, 162-168. <https://doi.org/10.1016/j.cemconcomp.2014.09.008>.
 35. Rao, K.D.; Pranav, P.; Anusha. (2011) Stabilization of expansive soil with rice husk ash, lime and gypsum—an experimental study. *Int. J. Eng. Sci. Tech.* 3 [11], 8076-8085.
 36. Cizer, Ö.; Balen, K.V.; Elsen, J.U.; Gemert, D.V. (2006) Carbonation and hydration of calcium hydroxide and calcium silicate binders with rice husk ash. In: 2nd International RILEM Symposium, Rilem Publications SARL, France. 611.
 37. Nguyen, V.T.; Ye, G.A.; van Breugel, K.; Fraaij, A.L.A.; Bui, D.D. (2011) The study of using rice husk ash to produce ultra high performance concrete. *Constr. Build. Mater.* 25 [4], 2030-2035. <https://doi.org/10.1016/j.conbuildmat.2010.11.046>.
 38. Ahsan, M.B.; Hossain, Z. (2018) Supplemental use of rice husk ash (RHA) as a cementitious material in concrete industry. *Constr. Build. Mater.* 178, 1-9. <https://doi.org/10.1016/j.conbuildmat.2018.05.101>.

39. GB/T 51003-2014 (2014) Technical code for application of mineral admixture. Standardization Administration of China, Beijing, China.
40. Nguyen, V. (2011) Rice husk ash as a mineral admixture for ultra-high performance concrete. PhD, Delft University of Technology, Netherlands, 2011.
41. Yu, Q.J.; Sawayama, K.; Sugita, S.; Shoya, M.; Isojima, Y. (1999) The reaction between rice husk ash and $\text{Ca}(\text{OH})_2$ solution and the nature of its product. *Cement Concrete Res.* 29 [1], 37-43. [https://doi.org/10.1016/S0008-8846\(98\)00172-0](https://doi.org/10.1016/S0008-8846(98)00172-0).